Hofstadter butterfly fractals and their topological properties

Mengjie Yang[1, *]

[1] *Department of Physics, National University of Singapore, Singapore 117551, Singapore*

(Dated: November 17, 2023)

We begin with a minimal tight-binding model that includes a magnetic flux and apply the Landau gauge to obtain the Harper equation. The Harper equation is a one-dimensional Schrödinger equation with a periodic potential, whose numerical solution reveals the fractal energy spectrum known as the Hofstadter butterfly. We then explore the band topology of this system by imposing open boundary conditions along the x direction and periodic boundary conditions along the y direction. We demonstrate the remarkable effect of the topology by studying the edge dynamics, where we observe the wavepacket moving along the boundaries of the square lattice in either clockwise or counter-clockwise directions, depending on the resonant external source. Finally, we introduce the concepts of Berry curvature and Chern number, and provide some references for their computation.

I. INTRODUCTION

Hofstadter's butterfly is a visualization of the spectral characteristics of non-interacting electrons confined to a two-dimensional lattice subjected to a perpendicular magnetic field. The intricate and self-replicating, i.e., fractal, structure of this spectrum was first unveiled during Douglas Hofstadter's doctoral research in 1976 and stands as a milestone [1]. The term "butterfly" originates from Hofstadter's description, in which he noted that the significant voids within the graph create a captivating pattern that somewhat resembles the shape of a butterfly [1]. The Hofstadter butterfly reveals the complex interplay between the periodic potential of the lattice and the magnetic field, which leads to the formation of Landau levels and the quantum Hall effect. The spectrum can be understood as a function of the magnetic flux per plaquette, which is usually expressed as a rational fraction $\alpha = p/q$, where p and q are coprime integers. For each value of α, the original Bloch band splits into q subbands, which are separated by gaps of different sizes.

One of the remarkable features of the Hofstadter butterfly is that it encodes the topological properties of the system, which can be characterized by the Chern numbers of the subbands. The Chern number is a topological invariant that measures the Berry curvature integrated over the Brillouin zone. It determines the quantized Hall conductance of the system, as well as the number and chirality of the edge states that appear when the system has a finite size and open boundary conditions. The edge states are topologically protected from backscattering and localization, and they can transport charge and spin along the boundary of the system [2]. The Hofstadter butterfly thus provides a rich platform to study the physics of topological phases and edge modes in two-dimensional systems.

To understand the Hofstadter butterfly better, this report is organized as follows: In Sec. II, we start with a minimal tight-binding model featuring a magnetic flux and derive the Harper equation by applying the Landau gauge. This equation represents a one-dimensional Schrödinger equation characterized by a periodic potential. Numerical solutions of the Harper equation reveal an energy spectrum that manifests as Hofstadter butterfly fractals. Moving on to Sec. III, we explore the band topology within this system under open boundary conditions along the x direction and periodic boundary conditions along the y direction. To observe the intriguing effects of the topology, we delve into the study of edge dynamics, tracking the movement of wave packets along the boundaries of the square lattice. In Sec. IV, we introduce the concepts of Berry curvature and the Chern number, providing references for their calculation. Finally, our findings are summarized in Sec. V.

II. HOFSTADTER BUTTERFLY IN A SQUARE LATTICE

A tight-binding model corresponding to a square lattice with a magnetic flux of b per plaquette can be written as

$$H = -t \sum_{\langle i,j \rangle} e^{i\phi_{ij}} c_i^\dagger c_j, \tag{1}$$

where t is the hopping amplitude, $\langle i,j \rangle$ denotes nearest-neighbor pairs, $c_i^\dagger$ and c_j are the creation and annihilation operators of electrons on sites i and j, and ϕ_{ij} is the phase acquired by the electron when hopping from site i to site j due to the magnetic field. The phase ϕ_{ij} is related to the vector potential $\mathbf{A}$ by

$$\phi_{ij} = \frac{q}{\hbar} \int_i^j \mathbf{A} \cdot d\mathbf{l}, \tag{2}$$

where q is the charge of the electron and $\hbar$ is the reduced Planck constant.

To simplify the problem, we can choose the Landau gauge $\mathbf{A} = (0, Bx, 0)$, where B is the magnetic field strength. In this gauge, the phase ϕ_{ij} depends only on

* mengjie.yang@u.nus.edu

the x-coordinate of the initial site i. We can label the sites by their x and y coordinates as (x, y), where x and y are integers. The lattice constant is set to $a = 1$ for convenience. The magnetic flux per plaquette is then given by

$$\alpha = \frac{Ba^2}{\Phi_0} = \frac{B}{\Phi_0}, \tag{3}$$

where $\Phi_0 = h/q$ is the flux quantum.

In the Landau gauge, the Hamiltonian can be written as

$$\begin{aligned} H = &- t \sum_{x,y} \left(e^{i2\pi\alpha x} c^\dagger_{x,y} c_{x,y+1} + e^{-i2\pi\alpha x} c^\dagger_{x,y+1} c_{x,y} \right) \\ &- t \sum_{x,y} \left(c^\dagger_{x,y} c_{x+1,y} + c^\dagger_{x+1,y} c_{x,y} \right). \end{aligned} \tag{4}$$

The eigenstates of H in the form

$$\psi_{l,k} = \sum_{x,y} e^{ik_y} \psi_{l,x} \delta_{x-l,y}, \tag{5}$$

where l labels the approximate horizontal position of the eigenstate, k is the lattice momentum in the vertical direction, and $\delta_{x,y}$ is the Kronecker delta. Substituting this ansatz into the Schrödinger equation $H\psi_{l,k} = E\psi_{l,k}$, we obtain

$$H\psi_{l,k} = -t \sum_{x,y} e^{ik_y} \left(e^{i2\pi\alpha x} \psi_{l,x} \delta_{x-l,y+1} + e^{-i2\pi\alpha x} \psi_{l,x} \delta_{x-l,y-1} + \psi_{l,x} \delta_{x-l+1,y} + \psi_{l,x} \delta_{x-l-1,y} \right) = E \sum_{x,y} e^{ik_y} \psi_{l,x} \delta_{x-l,y}. \tag{6}$$

Simplifying the summation over y, we get

$$\begin{aligned} &- t \sum_x \left(e^{i2\pi\alpha x} \psi_{l,x} e^{ik} + e^{-i2\pi bx} \psi_{l,x} e^{-ik} \right) \\ &- t \sum_x \left(\psi_{l,x+1} + \psi_{l,x-1} \right) = E \sum_x \psi_{l,x}. \end{aligned} \tag{7}$$

Comparing the coefficients of $\psi_{l,x}$, we arrive at the desired relation, which is actually the well-known Harper equation:

$$2\psi_{l,x} \cos(2\pi\alpha x - k) + \psi_{l,x+1} + \psi_{l,x-1} = \epsilon_l(k) \psi_{l,x}, \tag{8}$$

where $\epsilon_l(k) = E/t$ is the dimensionless eigenenergy. Now we can see special phase factors when the electron hops between the atomic sites. The electron only gains phase factor hopping along the y-axis due to the Landau gauge.

Here, note that if α values are equal to p/q (p and q are the integers), α values are rational. And q values determine the matrix of size. The wavefunctions $\psi_{l,x}$ should obey the Bloch theorem, i.e., $\psi_{l,x+q} = e^{ikq} \psi_{l,x}$, where k is the lattice momentum in the vertical direction. Therefore, we can rewrite Eq. (8) in a matrix form as

$$\mathcal{H} = \begin{pmatrix} 2\cos(k_y - 2\pi\alpha) & 1 & 0 & \cdots & 0 & e^{-qikx} \\ 1 & 2\cos(k_y - 4\pi\alpha) & 1 & \cdots & 0 & 0 \\ 0 & 1 & 2\cos(k_y - 6\pi\alpha) & \cdots & 0 & 0 \\ \vdots & \vdots & \vdots & \ddots & \vdots & \vdots \\ 0 & 0 & 0 & \cdots & 2\cos(k_y - 2\pi(q-1)\alpha) & 1 \\ e^{qikx} & 0 & 0 & \cdots & 1 & 2\cos(k_y - 2\pi q\alpha) \end{pmatrix} \tag{9}$$

where the eigenenergy can be obtained from solving the eigensystems of $\mathcal{H}$ matrix above.

The Hofstadter butterfly thus can be plotted accordingly, as shown in Fig. 1. The x axis relates to the magnetic α, and the y axis corresponds to the eigenenergies. The fractals are self-similar, which means that the fractals are similar to each other at different scales. And fractals features can be observed obviously in the butterflies plotted in Fig. 1.

III. EDGE DYNAMICS IN THE HOFSTADTER BUTTERFLY

Fig. 2 illstrates the band structure calculated from Eq. (9) for our square lattice which is truncated to $N_x = 20$ sites in the x direction, while keeping periodic boundary conditions in the y direction, with the magnetic flux related to $p = 1$, (a) $q = 3$, (b) $q = 4$, (c) $q = 5$, and (d) $q = 6$. It can be seen that q indicates

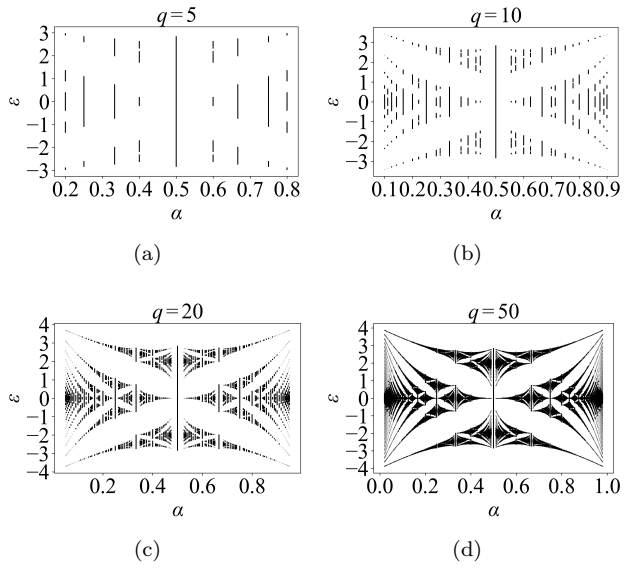

Figure 1. Hofstadter butterfly fractals for different q values, including (a) $q = 5$, (b) $q = 10$, (c) $q = 20$, and (d) $q = 50$. $p = 0, 1, ..., q$. q depicts the number of the bands. The x axis relates to the magnetic α, and the y axis corresponds to the dimensionless eigenenergies.

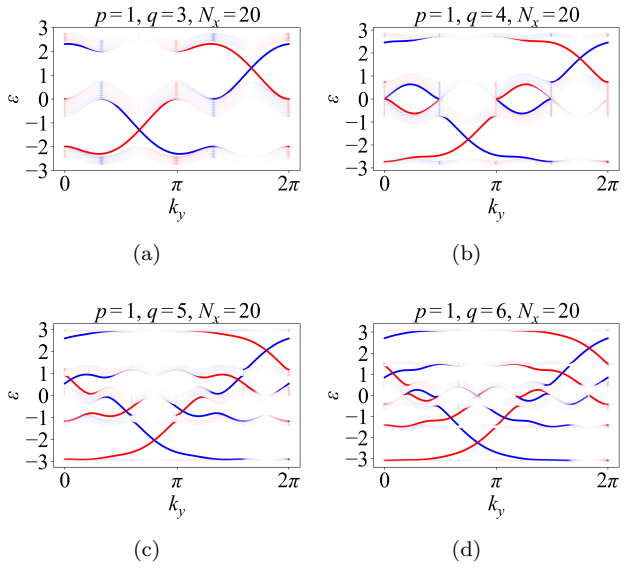

Figure 2. The band structure for our square lattice which is truncated to $N_x = 20$ sites in the x direction, while keeping periodic boundary conditions in the y direction, with the magnetic flux related to (a) $(p, q) = (1, 3)$, (b) $(p, q) = (1, 4)$, (c) $(p, q) = (1, 5)$, and (d) $(p, q) = (1, 6)$. q indicates the number of bands. We clearly observe bulk bands in light white and edge bands in red (right edge) and blue (left edge) due to the nontrivial topology caused by the magnetic field.

the number of bands. Furthermore, we clearly observe bulk bands (in light white colors) and edge bands, blue and red, due to the nontrivial topology caused by the magnetic field. The blue topological bands indicate the eigenstate localization is on the left edge of the lattice, while the red topological bands indicate the eigenstate localization is on the right edge of the lattice.

Now, for studying the edge dynamics, if we both truncate the x and y direction, we can see the double open boundary conditions spectrum in Fig. 3(a), where we use $p = 1, q = 3$. The number on each direction is 20, i.e., $N_x = N_y = 20$. We already see in-gap topological states connecting three bulk bands, which also can be verified in Fig. 2(a). The bulk and topological eigenstate loclaization distributions are also shown in Fig. 3. The eigenstate distribution of the $n = 1, \epsilon = -2.72$ eigenstate, which corresponds to bulk states, is shown in Fig. 3(b). The eigenstate distribution of the $n = 396, \epsilon = -1.57$ or $n = 805, \epsilon = +1.57$ eigenstate, which is an illustration of topological edge states, is shown in Fig. 3(c) or (d). We can see that the edge states are localized at the four boundaries of the square lattice.

To see the dynamics of edge states, we first have a try by putting an initial state (non-driven) on the center of the first row, i.e., $\mathbf{r}$ is $(x = 10, y = 1)$. What we observe is that the wavepacket moves along the cloclwise and counter-clockwise directoins at the same time, as in Fig. 4. Also, the propagation is rather messy as time goes by. Nevertheless, we still observe the wavepacket moving along the boundaries of the square lattice.

On the other hand, to enhance the performances of the edge dyanmics and prevent it being affected by bulk propagation, we simulate the system by an external countinuous source $\eta(\mathbf{r}, t) = \eta_0 e^{-i\epsilon_s t}\delta_{\mathbf{r},\mathbf{r}_s}$, which is localized at $\mathbf{r} = \mathbf{r}_s$, the center of the first row, i.e., $\mathbf{r} = (x = 10, y = 1)$. The source excitation is with $\eta_0 = 1$ and $\epsilon_s = -1.57$ or $+1.57$. The snapshots of the counter-clockwise and clockwise dynamics are shown in Fig. 5 and Fig. 6, respectively. We can see that the wavepacket moves along the boundaries of the square lattice, and the propagation is much more clear than the non-driven case.

Interestingly, we further observe dominant counter-clockwise and clockwise dynamics in Fig. 5 and Fig. 6, respectively. The counter-clockwise dynamics is resonated with the topological modes on the right of the energy plane, as shown in Fig. 3(a) and (d). The clockwise dynamics is resonated with the topological modes on the left of the energy plane, as shown in Fig. 3(a) and (c). Though through Fig. 2(a), we find that for positive and negative energy, there are possibilities for both moving directions. However, the dominant moving direction is still determined by one of the directions, i.e., clockwise or counter-clockwise.

IV. THE CALCULATION OF BERRY CURVATURE AND CHERN NUMBER

Chern numbers play a crucial role in quantifying the topological aspects of conduction in the quantum Hall effect [3]. These numbers emerge as a fundamental part

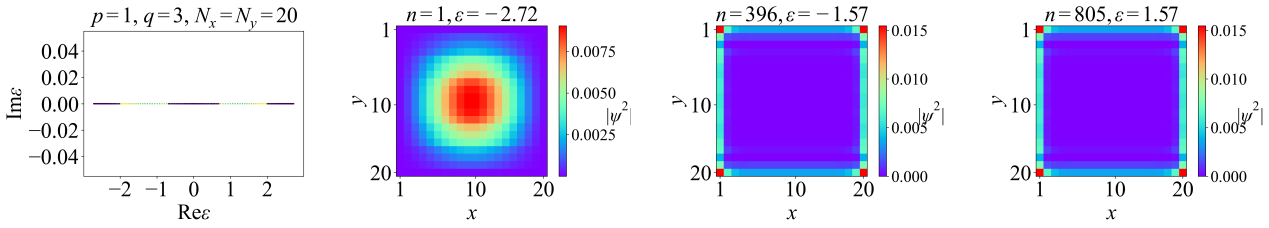

Figure 3. (a) The spectrum of the tight-binding model in Eq. (9) with open boundary conditions imposed on both x and y directions, where we use $p = 1, q = 3$. The number on each direction is 20, i.e., $N_x = N_y = 20$. We already see in-gap topological states (light green) connecting three bulk bands (dark purple), which also can be seen in Fig. 2(a). (b) The eigenstate distribution of the $n = 1, \epsilon = -2.72$ eigenstate, which corresponds to bulk states. (c) The eigenstate distribution of the $n = 396, \epsilon = -1.57$ eigenstate, and (d) $n = 805, \epsilon = +1.57$ eigenstate, which are illustrations of topological edge states.

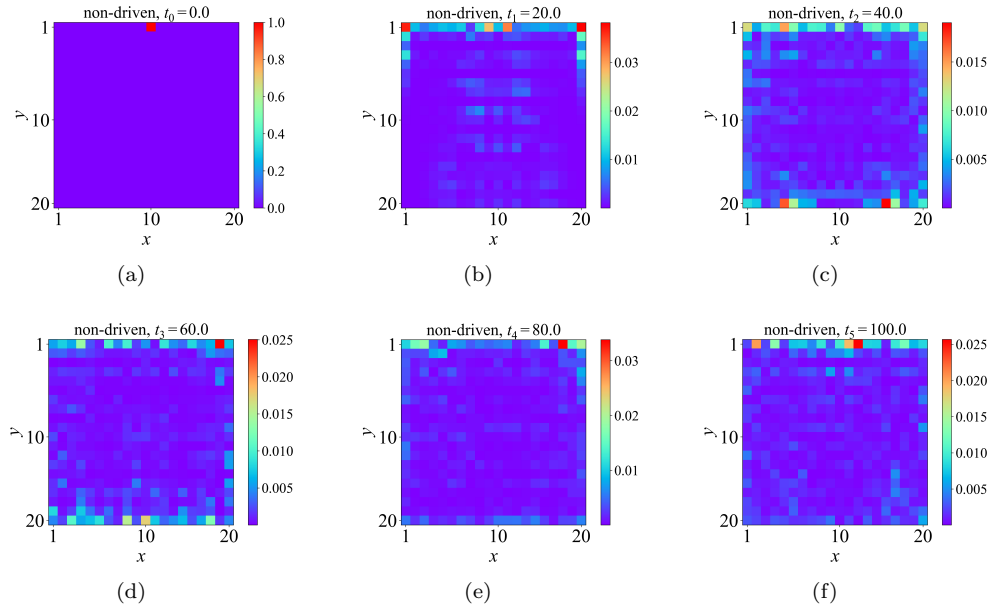

Figure 4. The snapshots of dynamics in non-driven case, where the initial state is a Gaussian wavepacket centered at the center of the first row ($y = 1$) of the square lattice. The snapshots are taken at time (a) $t_0 = 0$, (b) $t_1 = 20$, (c) $t_2 = 40$, (d) $t_3 = 60$, (e) $t_4 = 80$, and (f) $t_5 = 100$.

of the experimental manifestation of the quantum Hall effect and are a necessity for any effective theory describing this phenomenon. While the Thouless-Kohmoto-Nightingaleden Nijs (TKNN) formula allows for analytical determination of Chern numbers in certain scenarios [4], the complexity of Hamiltonians in more intricate cases can render analytical solutions unattainable. C_j is the Chern number that is summed over j occupied bands in the Brillouin zone and is defined as

$$C_n = \frac{1}{2\pi} \int_{BZ} \Omega_n(\mathbf{k}) d^2\mathbf{k}, \tag{10}$$

where $\Omega_n(\mathbf{k})$ is the Berry curvature of the n-th band, which is defined as

$$\Omega_n(\mathbf{k}) = i \left(\langle \partial_{k_x} u_{n,\mathbf{k}} | \partial_{k_y} u_{n,\mathbf{k}} \rangle - \langle \partial_{k_y} u_{n,\mathbf{k}} | \partial_{k_x} u_{n,\mathbf{k}} \rangle \right), \tag{11}$$

where $u_{n,\mathbf{k}}$ are Bloch states calculated by Hamiltonian. (9). The Chern number is an integer that characterizes the topological properties of the band. If the Chern number is non-zero, the band is topologically non-trivial, whereas the Chern number is zero for trivial bands [5].

Obtaining numerical solutions for Chern numbers holds significant importance in comprehending the dynamics of intricate systems and novel models characterized by more complex Hamiltonians. In a 2005 paper by Fukui et. al., a novel approach for the numerical computation of Chern numbers was introduced [6].

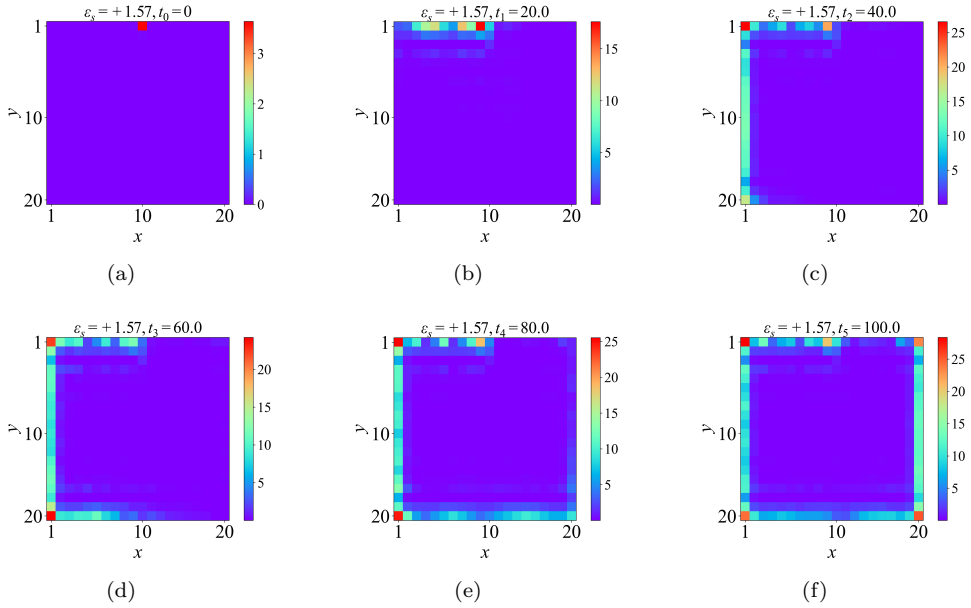

Figure 5. The snapshots of counter-clockwise dynamics in the continuously driven case, where the excited frequency $\epsilon_s = +1.57$ is resonated with the topological modes on the right of the energy plane, as shown in Fig. 3(a) and (c). The position of the external source is on the center of the first row of the square lattice, i.e. $x = 10, y = 1$. The snapshots are taken at time (a) $t_0 = 0$, (b) $t_1 = 20$, (c) $t_2 = 40$, (d) $t_3 = 60$, (e) $t_4 = 80$, and (f) $t_5 = 100$.

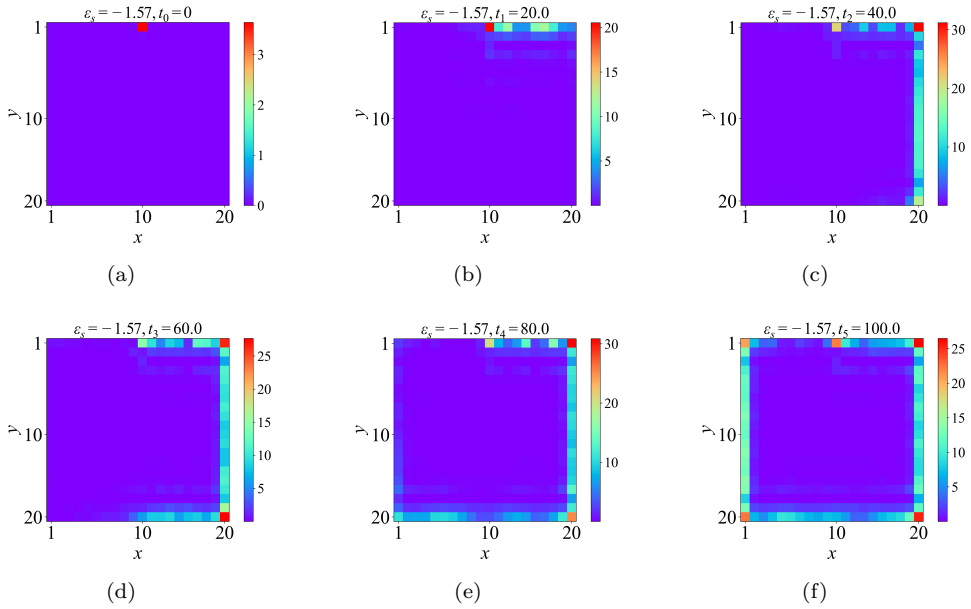

Figure 6. The snapshots of clockwise dynamics in the continuously driven case, where the excited frequency $\epsilon_s = -1.57$ is resonated with the topological modes on the left of the energy plane, as shown in Fig. 3(a) and (c). The position of the external source is on the center of the first row of the square lattice, i.e. $x = 10, y = 1$. The snapshots are taken at time (a) $t_0 = 0$, (b) $t_1 = 20$, (c) $t_2 = 40$, (d) $t_3 = 60$, (e) $t_4 = 80$, and (f) $t_5 = 100$.

A. Definition of Chern number

In our system, let us consider a two-dimensional system, where the Brillouin zone is defined by:

$$0 < k_1 < 2\pi/q_1, 0 < k_2 < 2\pi/q_2, \text{where } q_1, q_2 \text{ are integers.} \tag{12}$$

The Chern Number, is an integer, as proven in the Chern-Gauss-Bonnet Theorem. The Chern Number may be considered as a sum of "patches" over the Brillouin Zone. For these patches, by Stokes Theorem, the only significant contribution is the boundary. This bound-

ary gives a winding number, $(\theta_f - \theta_i)/(2\pi)$, for a given $U(1)$ transformation $(|n(k)\rangle \to \left(e^{i\lambda(k)}|n(k)\rangle\right)$, around the patch. The winding number around a closed loop is necessarily and integer. Thus, taking the limit where the patches become small, the Chern Number may be calculated as a momentum-space integral over the Brillouin zone over the "Berry curvature," $F(k)$:

$$c_n = \frac{1}{2\pi i}\int_{BZ} d^2k F(k) \tag{13}$$

The Berry curvature, or field strength, may be calculated from the Berry connection $A(k)$:

$$F(k) = \frac{\partial}{\partial k_1}A_2(k) - \frac{\partial}{\partial k_2}A_1(k) \tag{14}$$

Where the Berry connection, or gauge potential, is found from the wave functions $|n(k)\rangle$:

$$A_i(k) = \left\langle n(k)\left|\frac{\partial}{\partial k_i}\right|n(k)\right\rangle \tag{15}$$

The normalized wave functions of the n-th Bloch band, $E_n(k)$, are $|n(k)\rangle$ such that:

$$H(k)|n(k)\rangle = E_n(k)|n(k)\rangle \tag{16}$$

B. Commonly used method for calculating Chern number

The numerical analysis of wave functions is based upon the evaluation of the wave functions at finitely many locations in the Brillouin Zone. Now, recall that the derivative is defined as the limit of finite differences:

$$f'(x) = \lim_{h\to 0}\frac{f(x+h) - f(x)}{h} \tag{17}$$

In this discretized scheme, the wave functions $|n(k)\rangle$ are equivalent, but only defined at finitely many points. Let these points be, for small δk_1, and δk_2 :

$$\begin{aligned} k_1 &= \{0, \delta k_1, 2\delta k_1, \ldots, 2\pi/q_1 - \delta k_1\} \\ k_2 &= \{0, \delta k_2, 2\delta k_2, \ldots, 2\pi/q_2 - \delta k_2\} \end{aligned} \tag{18}$$

It is then possible to compute the Berry connection, with $\delta_i f(k) \equiv f\left(k + \delta k_i\right) - f(k)$:

$$A_i(k) = \left\langle n(k)\left|\frac{\delta_i}{\|\delta k_i\|}\right|n(k)\right\rangle \tag{19}$$

From there, the Berry curvature may be calculated as:

$$F(k) = \frac{\delta_1}{\|\delta k_1\|}A_2(k) - \frac{\delta_2}{\|\delta k_2\|}A_1(k) \tag{20}$$

Next, note that numeric integration in two dimensions may be computed as a sum over points $f\left(x_{1,i}, x_{2,j}\right)$:

$$\int_{a_1}^{b_1} dx_1 \int_{a_2}^{b_2} dx_2 f\left(x_1, x_2\right) = \lim_{\Delta x_{1,2}\to 0}\sum_i \Delta x_1 \sum_j \Delta x_2 f\left(x_{1,i}, x_{2,j}\right) \tag{21}$$

The Chern number may then be calculated as a sum over k_1 and k_2, in the limit of δk_1 and δk_2 small:

$$c_n = \frac{1}{2\pi i}\sum_{k_1}\delta k_1 \sum_{k_2}\delta k_2 F\left(k_1, k_2\right) \tag{22}$$

This algorithm is most accurate when δk_1 and δk_2 are small.

C. Fukui-Hatsugai-Suzuki method

Begin by specifying that in the Brillouin zone, k_1 may be divided into N_1 pieces, and k_2 may be divided into N_2 pieces. Next, specify the increment lengths $\delta k_1 = 2\pi/q_1 N_1$, and $\delta k_2 = 2\pi/q_2 N_2$. Now, if $j_1 = \{0, 1, \ldots, N_1 - 1\}$, and $j_2 = \{0, 1, \ldots, N_2 - 1\}$, the position of a discretized point may be specified as [7]: $k = (\delta k_1 j_1, \delta k_2 j_2) \equiv (j_1, j_2)$ where δk_1 and δk_2 are dropped for notational simplicity.

Recall that the Hamiltonian is periodic, so from Bloch's theorem, the wave functions can be assumed periodic:

$$\begin{aligned} |n\left(j_1, j_2\right)\rangle &= |n\left(j_1 + N_1, j_2\right)\rangle \\ &= |n\left(j_1, j_2 + N_2\right)\rangle \end{aligned} \tag{23}$$

Next, define a "link variable" about one point

$$U_1\left(j_1, j_2\right) \equiv \frac{\langle n\left(j_1, j_2\right) \mid n\left(j_1 + 1, j_2\right)\rangle}{\|\langle n\left(j_1, j_2\right) \mid n\left(j_1 + 1, j_2\right)\rangle\|} \tag{24}$$

and

$$U_2\left(j_1, j_2\right) \equiv \frac{\langle n\left(j_1, j_2\right) \mid n\left(j_1, j_2 + 1\right)\rangle}{\|\langle n\left(j_1, j_2\right) \mid n\left(j_1, j_2 + 1\right)\rangle\|} \tag{25}$$

An analogue to the Berry curvature is defined as:

$$\widetilde{F}\left(j_1,j_2\right)\equiv\ln\left(\frac{U_1\left(j_1,j_2\right)U_2\left(j_1+1,j_2\right)}{U_1\left(j_1,j_2+1\right)U_2\left(j_1,j_2\right)}\right) \tag{26}$$

The Chern Number is then calculated as a sum over all sites (j_1, j_2) as:

$$c_n=\frac{1}{2\pi i}\sum_{j_1,j_2}\widetilde{F}\left(j_1,j_2\right) \tag{27}$$

If $N_1 = q_2N_B$ and $N_2 = q_1N_B$, then the unit plaquette is square. This algorithm is most accurate when N_B is large. In particular Fukui reports that Chern Numbers are accurate when $N_B \geq \mathcal{O}\left(\sqrt{2\left|c_n\right|/\left(q_1q_2\right)}\right)$.

D. The calculation of non-Abelian Berry curvature and Chern number in our system

In the previous section, we have introduced the commonly used method for calculating the Chern number. However, the commonly used method is more convenient for the Abelian Berry curvature. In our system, the Berry curvature is non-Abelian, since the bands are not separated by gaps.

For the compuation of the non-Abelian Berry curvature, one possible approach is to use the Wilson loop approach [8]. Wilson loop approach is a nice tool to calculate the topological invariant, which is gauge invariant and compatible with numerical implementations. The method is quite general and can be used to describe both tight-binding models [9] and continuous models [10]. It is also convenient to use it to describe multi-band system. Here we probide the concept of the Wilson loop and then apply it to describe the topological properties of the breathing honeycomb lattice. Considering a matrix $M^{k_i,k_{i+1}}$, whose elements are obtained by

$$M_{n,n'}^{k_i,k_{i+1}}=\langle u^{n,k_i}|u^{n',k_{i+1}}\rangle, \tag{28}$$

where n and n' are band indices covering all the N bands below the concerned band gap, and k_i, k_{i+1} are two closer points on a loop in Brillouin zone. The Wilson loop can be obtained from the matrix product of a class of $M^{k_i,k_{i+1}}$,

$$W=\prod_i M^{k_i,k_{i+1}}. \tag{29}$$

where $k_1, k_2, ..., k_N$ from a closed loop in the Brillouin zone. For the one-dimensional problem, the Berry phases of each band are given by

$$\theta_n=i\log w_n \tag{30}$$

where w_n are the eigenvalues of W. For higher-dimensional systems, we can consider the Berry phase along one direction $k_{||}$ as a function of $k_\perp$, i.e., $\theta_n(k_\perp)$. For example, the well-known Chern number in two-dimensional system can be obtained by the winding of $\theta_n(k_y)$ as

$$\begin{aligned}2\pi C_n&=-\int_{-\pi}^{\pi}\int_{-\pi}^{\pi}\mathrm{d}k_x\ \mathrm{d}k_y\left(\partial_{k_x}\mathcal{A}_n^y-\partial_{k_y}\mathcal{A}_n^x\right)\\&=\int_{-\pi}^{\pi}\mathrm{d}k_y\partial_{k_y}\left(\int_{-\pi}^{\pi}\mathrm{d}k_x\mathcal{A}_n^x\right)\\&=\int_{-\pi}^{\pi}\mathrm{d}\theta_n\left(k_y\right).\end{aligned} \tag{31}$$

where $\theta_n(k_y)$ is the Berry phase calculated from the one-dimensional integration of $A_n^x(k_x, k_y)$ along the k_x direction for each fixed k_y.

V. DISCUSSIONS

In this report, we have studied the topological properties of a square lattice in a magnetic field, which plays a key role in generating non-trivial band topology. By computing the Berry curvature and Chern numbers of the bands, we have characterized the topological phases of the system. Furthermore, we have investigated the edge dynamics of the system, which exhibit localized states at the boundaries of the square lattice. These edge states can be excited by an external source and propagate along the boundaries in a direction determined by the frequency of the source. Our results demonstrate the rich physics of topological insulators in a simple tight-binding model.

[1] D. R. Hofstadter, Energy levels and wave functions of bloch electrons in rational and irrational magnetic fields, Physical review B **14**, 2239 (1976).

[2] Y. Hatsugai, Chern number and edge states in the integer quantum hall effect, Physical review letters **71**, 3697 (1993).

[3] M. E. Cage, K. Klitzing, A. Chang, F. Duncan, M. Haldane, R. B. Laughlin, A. Pruisken, and D. Thouless, *The quantum Hall effect* (Springer Science & Business Media, 2012).

[4] D. J. Thouless, M. Kohmoto, M. P. Nightingale, and M. den Nijs, Quantized hall conductance in a two-

dimensional periodic potential, Physical review letters **49**, 405 (1982).
[5] M. Z. Hasan and C. L. Kane, Colloquium: topological insulators, Reviews of modern physics **82**, 3045 (2010).
[6] T. Fukui, Y. Hatsugai, and H. Suzuki, Chern numbers in discretized brillouin zone: efficient method of computing (spin) hall conductances, Journal of the Physical Society of Japan **74**, 1674 (2005).
[7] A. Dauphin, M. Müller, and M. A. Martin-Delgado, Efficient algorithm to compute the berry conductivity, New journal of physics **16**, 073016 (2014).
[8] X. Zhang, Y. Chen, Y. Wang, Y. Liu, J. Y. Lin, N. C. Hu, B. Guan, and C. H. Lee, Entangled four-dimensional multicomponent topological states from photonic crystal defects, Physical Review B **100**, 041110 (2019).
[9] A. Bouhon, A. M. Black-Schaffer, and R.-J. Slager, Wilson loop approach to fragile topology of split elementary band representations and topological crystalline insulators with time-reversal symmetry, Physical Review B **100**, 195135 (2019).
[10] H.-X. Wang, G.-Y. Guo, and J.-H. Jiang, Band topology in classical waves: Wilson-loop approach to topological numbers and fragile topology, New Journal of Physics **21**, 093029 (2019).